# Conformational Diversity of Short DNA Duplex

**S. Hicks, J. Case, and A. Jofre***

*Department of Physics and Optical Science, University of North Carolina Charlotte, Charlotte, North Carolina, United States*

*Received: April 9, 2010; Revised Manuscript Received: August 11, 2010*

Two 25 base-pair cDNA strands are encapsulated within an optically trapped nanodroplet, and we observe the kinetics of their hybridization in dynamic equilibrium via single-molecule fluorescence resonance energy transfer (FRET) as a function of temperature and of the solution's NaCl concentration. We have observed the duplex unfolding and refolding, and we have observed quasistable partially unfolded states under low salinity conditions. Furthermore, our measurements reveal that, even in conditions under which the duplex is stable, it undergoes conformational fluctuations in solution.

## 1. Introduction

The encapsulation of biomolecules within aqueous droplets is a widely accepted scheme for initiating and observing controlled chemical reactions. Biomolecules have been sequestered into aqueous droplets to observe single enzyme activity of $\beta$-D-galactosidase,[1] and more recently of chymotrypsin.[2] Devices have been developed to enable PCR within droplets,[3] and droplets have been used for cell-free synthesis of enhanced green fluorescent protein.[4] Recent work has also demonstrated that microdroplets suspended in mineral oil are functional bioreactors.[5]

Our work combines aqueous droplet sequestration of biomolecules with single-molecule methods. Our aqueous nanodroplets (hydrosomes) are under 1$\mu$m in diameter, which allows them to fit within a confocal fluorescence excitation spot. The hydrosomes are suspended in a fluorocarbon medium with an index of refraction lower than water, which enables them to be optically trapped. We use optical tweezers to hold the hydrosome within the confocal observation volume. A single molecule encapsulated within the droplet diffuses freely throughout the volume of the droplet but remains confined within the observation region, allowing for long observation times without physically attaching the molecule to the microscope coverslip. This allows for a different type of single-molecule study than what has been done before on DNA. Single-molecule measurements on the bonds between cDNA strands have previously been made by mechanically pulling the strands apart.[6] Other single-molecule measurements of DNA that bear more resemblance to our work have investigated conformational fluctuations on short time scales as the molecules diffuse through a confocal observation volume,[7,8] and single DNA hybridization events have been detected with DNA that is tethered to a coverslip surface.[9,10] However, this is the first single-molecule study of conformational fluctuations of DNA oligos in solution.

Recent studies have shown that short double-stranded DNA oligos exhibit a high degree of conformational flexibility on short scales along its length;[11,12] such flexibility may play a key role in interactions with proteins. For example, *Hha*I methyltransferase has been observed to deform DNA such that the cytosine base swings out of the DNA helix.[13] This phenomenon, known as base-flipping,[14,15] plays a key role in many processes in which enzymes need to access DNA bases, such as in DNA repair. Recent molecular dynamics simulations[16−18] have shown that such base-flipping can occur spontaneously for short DNA duplexes in solution.

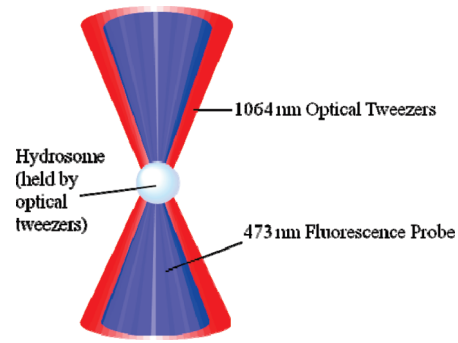


**Figure 1.** Conceptual schematic of the hydrosome technique for isolating and probing single molecules. An optical trap (depicted in red) holds a hydrosome containing a single molecule, and the molecule is probed by an overlapping blue laser.

Here we report our observations of conformational fluctuations of individual DNA duplexes in chemical equilibrium under various temperatures and salt concentrations.

**1.1. Hydrosome Technique for Single-Molecule Studies.** The two single strands of DNA under observation are isolated and encapsulated within an optically trapped femtoliter volume chemical container.[19] The container, which we call a hydrosome, is a stable aqueous nanodroplet (≈700 nm diameter) suspended in a low index-of-refraction fluorocarbon medium. The fluorocarbon medium is immiscible with water and has an index of refraction lower than that of water; therefore droplets ("hydrosomes") suspended in this medium are stable and optically trappable. A tightly focused infrared laser ("optical tweezers") holds a single hydrosome within a confocal observation volume created by a second laser, a visible probe beam, which fluorescently excites the molecule contained within the hydrosome. The fluorescence emission of the encapsulated molecule is collected by avalanche photodiodes and recorded until the molecule photobleaches. It has been shown in previous work[20,21] that the molecules sequestered within the hydrosome diffuse freely throughout its volume. Figure 1 shows a conceptual diagram of a hydrosome, containing a single molecule, held

* To whom correspondence should be addressed. E-mail: ajofre@uncc.edu.

10.1021/jp1032146 
Published on Web 10/28/2010

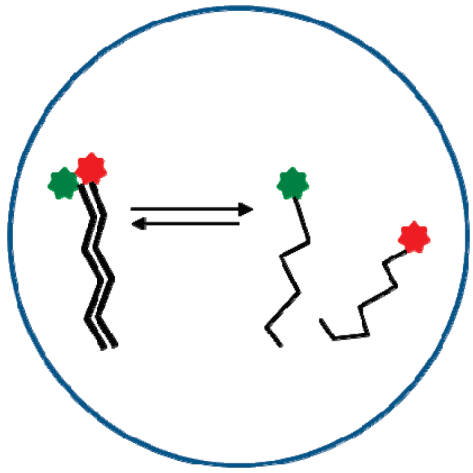

**Figure 2.** A cartoon illustration of the kinetics of two fluorescently labeled cDNA strands unbinding and rebinding within the confines of a hydrosome.

by optical tweezers within the confocal probing volume of a second focused laser.

## 2. Experiment Details

**2.1. Methodology and Materials.** Changes in structure and conformation are detected using single-molecule fluorescence resonance energy transfer (FRET). One fluorophore (the "donor") is attached to the 5′ end of the DNA oligo we call the probe, and the corresponding FRET fluorophore (the "acceptor") is attached to the 3′ end of the cDNA oligo we call the target. The FRET efficiency is expected to be at its highest when the two strands are bound in a B-form double helix. A change in distance between the two fluorophores, resulting from the DNA strands unbinding or from other fluctuations, is manifested as a change in the FRET efficiency.

The DNA sequences are 25 base-pairs long, have a 52% GC content, and have no secondary structure. The sequence of the probe is 5′ GCA TCT GGT ACT GAG TTA CAC CAC C 3′; the complementary target sequence is 5′ GGT GGT GTA ACT CAG TAC CAG ATC G 3′. The melting temperature of the sequence duplex at a 1 nM concentration is expected to be 57.8 °C when the concentration of NaCl is at 57 mM and 34.5 °C when the concentration of NaCl is at 5 mM.[22] The fluorophores used to label the DNA, Alexa 488 (the donor) and Alexa 594 (the acceptor), were attached to the ends of the oligos via 3-carbon linkers. Similar pairs of fluorophores have been observed to exhibit strong interactions with one another when placed in very close proximity.[23] To the best of our knowledge, no such interactions have been observed between Alexa 488 and Alexa 594. The Förster distance, $R_0$ (the distance at which the FRET efficiency is 0.5), for this pair of fluorophores is 57 Å. We first hybridize the DNA and then load it into our nanodroplets (hydrosomes), and expect to see kinetic fluctuations of the duplex under dynamic equilibrium at elevated temperatures and low salt concentrations. The cartoon in Figure 2 depicts a simple example of such kinetic fluctuations: the DNA unbinding and rebinding.

**2.2. Experimental Procedure and Equipment.** To prepare for the single-molecule measurements, we first hybridize the DNA before encapsulating the duplexes within the aqueous nanodroplets (hydrosomes). The DNA, purchased from IDT (Coralville, IA), is reconstituted in Tris−EDTA buffer (10 mM Tris, 1 mM EDTA, pH 8.0), purchased from Sigma-Aldrich (St. Louis, MO). We hybridized the DNA by mixing equal parts of the complementary strands in Tris−EDTA buffer at a concentration of 1 $\mu$M with 57 mM NaCl.

The hybridized DNA solution is diluted to a concentration of 1 nM with Tris−EDTA buffer, and the concentration of NaCl is adjusted to the desired environmental conditions. Lower salt concentrations are expected to destabilize the DNA duplex, as dissolved ions shield the charged phosphate groups that compose the DNA's backbone. To facilitate droplet formation, we add a small quantity (0.1% v/v) of the surfactant Triton X100, purchased from Sigma-Aldrich (St. Louis, MO), to the aqueous solution. The hydrophobic fluorocarbon, purchased as FC-40 from 3 M (St. Paul, MN), is purged with nitrogen prior to mixing it with the aqueous solution to expel dissolved oxygen, as oxygen is known to enhance the photobleaching rates of fluorescent molecules.[24−27] Ultrasonication of the mixture results in a water-in-oil emulsion with small (≈700 nm diameter) aqueous droplets suspended in the hydrophobic matrix, each containing an average of one molecule, where the distribution of molecules within the hydrosomes is Poissonian.

We examine each hydrosome individually. Hydrosomes containing more than one molecule are identified by multiple photobleaching steps in the photon count traces and thrown out. Similarly, empty hydrosomes will not yield any signal above background, and these data are also thrown out. Only single FRET pair data are kept for further analysis.

The prepared hydrosome emulsion is transferred into a microscope sample cell and placed onto an inverted microscope, which is equipped with a heater/cooler that maintains the sample at a fixed temperature to within 0.05 °C. The heating and cooling of the microscope sample cell is achieved by means of a thermoelectric (Peltier) element, purchased from TE Technology (Traverse City, MI). The sample's temperature is monitored using judiciously placed thermistors and controlled by means of a proportional-integral (PI) controller, also purchased from TE Technology.

A 5 W infrared laser at 1064 nm, purchased from IPG photonics (Oxford, MA), is used to optically trap an individual droplet, and the molecule it contains is probed using a 5 mW visible laser at 473 nm, purchased from CrystaLaser (Reno, NV). To avoid enhanced photobleaching in the presence of two laser fields,[28] the infrared trapping beam and visible probe beam are alternately turned on and off at a rate of 50 kHz using acousto-optic modulators. At 50 kHz, the switching is sufficiently rapid to keep the hydrosome trapped.[29]

The infrared optical tweezers are combined with the visible fluorescence excitation laser at a dichroic reflector and directed into a 1.3 numerical aperture objective. The fluorescence emission of the molecule is spectrally separated and collected by two avalanche photodiode detectors, purchased from PicoQuant (Berlin Germany). One detector collects light from the donor fluorophore in the spectral range of 500−550 nm, and the other detector collects light from the acceptor fluorophore in the spectral range of 580−700 nm.

**2.3. Data Analysis.** ***2.3.1. Data Processing and Filtering.*** The photons in each channel are counted in 20 $\mu$s bins, and we rebin the counts into 10 ms bins.

To better resolve distinct signal levels amid noise, we employ the use of a nonlinear filter,[30] which is based on a *sliding-window average*. In a simple sliding-window average, any filtered data point $i$ with a value $I(i)$ is calculated based upon the mean of the $N$ unfiltered data values immediately before or after it. Thus, a window of fixed width $N$ "slides" across the raw data from beginning to end, and the average of all data values within that window becomes the filtered value corresponding to either the

leading or trailing edge of the window. This is described mathematically as follows:

$$I^{f}(i) = \frac{1}{N}\sum_{j=i-N}^{i-1} I(j) \quad (1)$$

$$I^{b}(i) = \frac{1}{N}\sum_{j=i+1}^{i+N} I(j) \quad (2)$$

$I^{f}$ is the filtered value on the leading edge of the window, called the "forward predictor," and $I^{b}$ is the filtered value on the trailing edge, or the "backward predictor". Several forward and backward predictors are calculated for each point $i$ by varying the window size $N$. Each predictor is then assigned a weight based on how close the raw data in the respective window remains to the mean. In this manner, predictors that are based on windows containing state transitions do not contribute to the final filter value. The filter is therefore able to respond quickly to signal transitions by discarding the windows in which they occur and by emphasizing windows that have little deviation from the mean. Also, the weights are determined by looking at both the donor and acceptor channels. This ensures that acceptor−donor timing correlations are preserved. The expressions for forward and backward predictor weights of window size $N_k$ are as follows:

$$f_k(i) = C_f\left\{\sum_{j=0}^{M-1}[(I_d(i-j) - I^{f}_{d,k}(i-j))^2 + (I_a(i-j) - I^{f}_{a,k}(i-j))^2]\right\}^{-p} \quad (3)$$

$$b_k(i) = C_b\left\{\sum_{j=0}^{M-1}[(I_d(i+j) - I^{b}_{d,k}(i+j))^2 + (I_a(i+j) - I^{b}_{a,k}(i+j))^2]\right\}^{-p} \quad (4)$$

$M$ is a filter variable that determines the range—in both directions—over which the predictors are compared to the actual signal. Larger values of $M$ tend to smooth the result while reducing sensitivity to small, fast changes. The exponent $p$ increases the speed at which the filter responds to transitions, but at the cost of noise. Larger values of $p$ tend to reduce the number of windows that contribute to the final value, resulting in sharper transitions but more noise. The values of $C$ are simply chosen to normalize the weights under the following requirement:

$$\sum_{k=1}^{K}(f_k(i) + b_k(i)) = 1 \quad (5)$$

The final result of the filter is the weighted sum of all the predictor windows, given by the following:

$$I_d^{filter}(i) = \sum_{k=1}^{K}(f_k(i)I^{f}_{d,k} + b_k(i)I^{b}_{d,k}) \quad (6)$$

We note that ref 30 contains a typographical error: the weights for the backward predictors were incorrectly dependent on the deviation from mean in the region *before* the current point $i$, not after. That is, the equation for $b_k$ operated on the point $(i - j)$, not $(i + j)$.

Our implementation of the filter uses predictor window sizes of 0.1, 0.2, 0.4, and 0.8 s; and values of $M = 10$ and $p = 100$. After varying both the number and sizes of filter windows, these values were determined empirically to provide the best signal-to-noise ratio.

***2.3.2. FRET Efficiency Histograms.*** The FRET efficiency, given by

$$E = \frac{(S_a - XS_d - B_a)}{(S_a - XS_d - B_a) + (S_d - B_d)} \quad (7)$$

is calculated at each 10 ms time bin in the filtered data traces. $S_a$ and $S_d$ are the signals detected in the acceptor detector channel and in the donor detector channel, respectively, and $B_a$ and $B_d$ are the background signals in the acceptor and donor channels, respectively. The crosstalk, $X$, is the fraction of light from the donor that is detected by the acceptor detector. The crosstalk was measured directly using a high concentration of donor fluorophore only; it was found to be 0.03. Similarly, we measured the direct excitation of the acceptor fluorophore, and found it to be negligible. It should be noted that the FRET efficiency given in eq 7 assumes that the detection correlation factor $\gamma$,[31−33] which depends on the detector efficiencies and on the fluorescence quantum yields of the fluorophores, is equal to 1. Hence, we do not claim accuracy in the absolute FRET values stated here; rather, our interest lies in revealing the relative changes in FRET efficiency as the system evolves in time.

We vary the temperature of our sample from 30 to 50 °C and vary the concentration of NaCl from 0.1 to 57 mM. For each temperature/salinity combination, we collect a single-molecule fluorescence time trace of 50−100 individual molecules and compile the FRET efficiencies of each 10 ms time bin in each trace into a histogram.

## 3. Results

The relationship between FRET efficiency and intermolecular distance is given by

$$E = \frac{1}{1 + \left(\frac{r}{R_o}\right)^6} \quad (8)$$

where $r$ is the distance between the fluorophores and $R_o$ is the Forster distance, which among other things depends on the relative orientation between the two fluorophores, and on the spectral overlap between the absorption of the acceptor and the emission of the donor. Given this strong dependence on the fluorophore distance, FRET is used as an effective molecular ruler, with the efficiency dropping as the distance increases. In this experiment, the distance probed is the distance between the two DNA strands. It is well-known that salt concentration affects the stability of the DNA duplex;[34] a higher salt concentration lowers the free energy of the duplex as it shields the electrostatic repulsion between the negatively charged phosphate groups.[35] We therefore expect that, at low salt concentrations and higher temperatures, the strands will be more likely to separate.

Figure 3a shows a typical single molecule FRET trace of the DNA duplex at 30 °C in a solution with 57 mM NaCl, environmental conditions under which the duplex is stable.

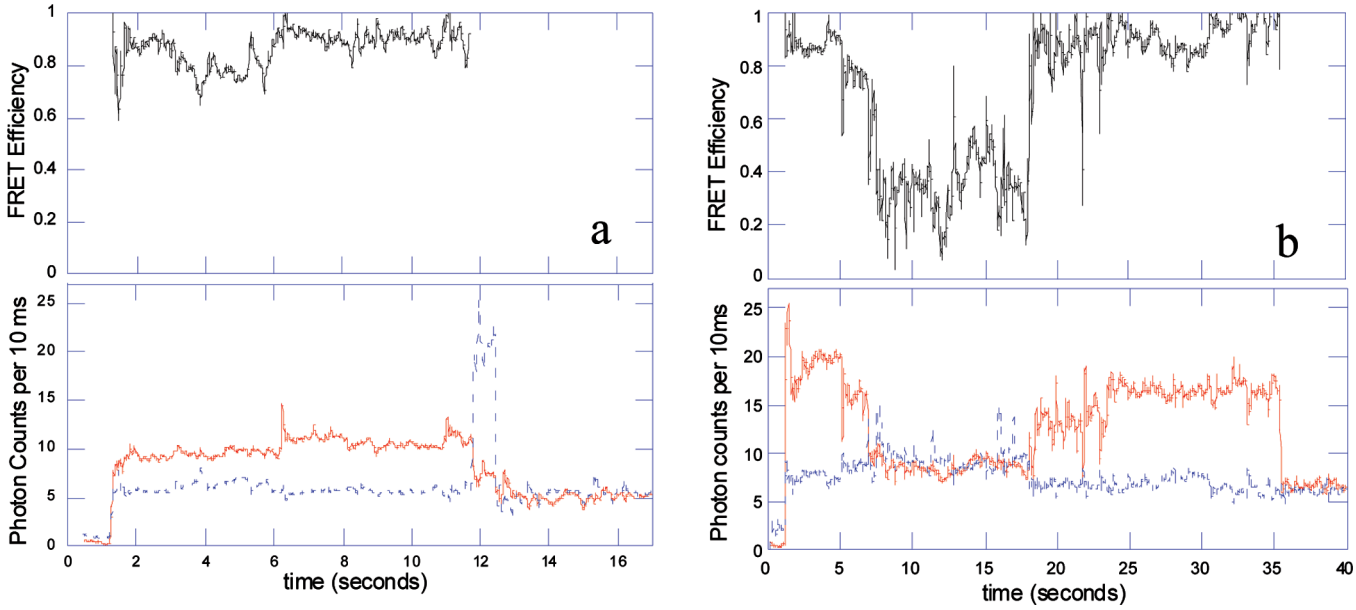


**Figure 3.** Single-molecule traces. Bottom traces: photon counts versus time. The solid red line is the acceptor; the dashed blue line is the donor. Top traces: The FRET efficiency versus time, corresponding to the data in the bottom traces. Environmental conditions: (a) 30 °C with 57 mM NaCl, and (b) 40 °C with 0.1 mM NaCl.

Although the FRET efficiency in this trace remains high, indicating that the distance between the DNA strands remain close, there is a clear fluctuation in the distance between the two strands.

For comparison, Figure 3b shows typical data traces at elevated temperatures and low NaCl concentration (40 °C and 0.1 mM of NaCl), conditions under which the DNA duplex is unstable, where one can see the large fluctuations in the FRET efficiency as a function of time. In this particular trace, the DNA partially unfolds and refolds, sampling an atypical state in which the separation between the fluorophores is roughly 60 Å.

The entire data set is summarized in the histograms of Figure 4, which show the FRET efficiency distributions for molecules at 30, 40, and 50 °C under two different concentrations of NaCl: 0.1 and 57 mM.

To better quantify the data, we applied a least-squares routine that fits each histogram to a function consisting of a sum of normal distributions, where each normal distribution represents a conformational state. For each histogram, we applied our least-squares fitting routine to six different models: (1) a sum of 2 normal distributions, (2) a sum of 3 normal distributions, (3) a sum of 4 normal distributions, (4) a sum of 5 normal distributions, (5) a sum of 6 normal distributions, and (6) a sum of 7 normal distributions.

To evaluate the fit of our data, we use the following figure of merit, which is not exactly the same as the traditional $\chi^2$:

$$\chi^2 = \frac{\sum_{j=1}^{N} (\text{data}(j) - \text{model}(j))^2}{\nu} \tag{9}$$

where $\nu$ is the number of degrees of freedom and $N$ is the total number of data points. In other words, we take the square sum of the errors and divide it by the number of degrees of freedom. The model that minimizes this figure of merit was chosen to best represent the data.

Explicitly, each histogram is fit to the following function:

$$f(x) = \sum_{i=1}^{n} A_i \exp\left(-\frac{(x - x_i)^2}{2\sigma_i^2}\right) \tag{10}$$

where $n$ indicates the number total number of normal distributions, $A_i$ is the amplitude of the $i$th distribution, $x_i$ is the mean of the $i$th distribution, and $\sigma_i$ is the root-mean-squared deviation of the $i$th distribution. The results of our fits are tabulated in Table 1.

The center point of each normal distribution corresponds to the mean FRET efficiency of a given conformational state, and the area under each normal curve represents the population fraction in that given conformational state. These results are summarized in Figure 5, which graphs the mean FRET efficiency versus the population fraction of the corresponding state.

After determining the number of conformational states and their mean FRET efficiency, we revisited each single molecule time trace to calculate the mean dwell time in each conformational state. The mean dwell time in each conformation is tabulated in Table 2 to a resolution of 10 ms.

## 4. Discussion

Interestingly, in Figure 4, at 40 °C with 0.1 mM of NaCl, the histogram indicates that a few specific distances are repeatedly sampled. We expect that, for completely random thermal fluctuations, the fluorophores that are attached to the ends of the DNA strands will sample many distances resulting in a broad distribution. This is observed in the situation at 40 °C with 57 mM of salt, where we suspect that the broad normal distribution centered at a FRET efficiency of 0.38 does not represent a single conformation but rather a variety of thermal fluctuations.

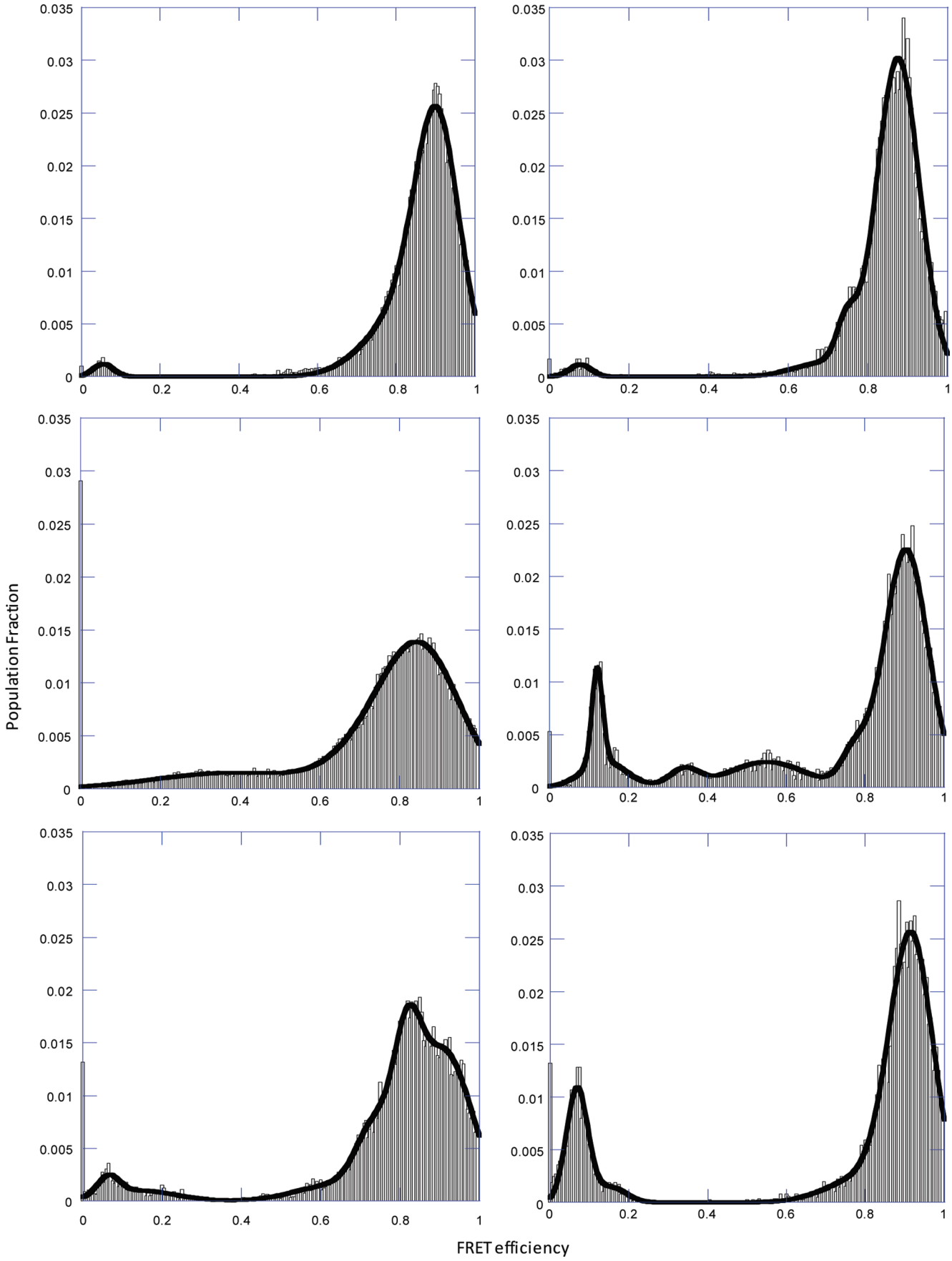


**Figure 4.** FRET efficiency histograms. FRET efficiency is on the *x*-axis, and the probability is on the *y*-axis. The solid line is the best fit to the data. Left, 57 mM NaCl; right, 0.1 mM NaCl. Top, 30 °C; middle, 40 °C; bottom, 50 °C.

We acknowledge the possibility that most of the DNA's conformational fluctuations occur on a shorter time scale than our 10 ms resolution. Given this limited temporal resolution, each normal distribution is in principle open to be interpreted

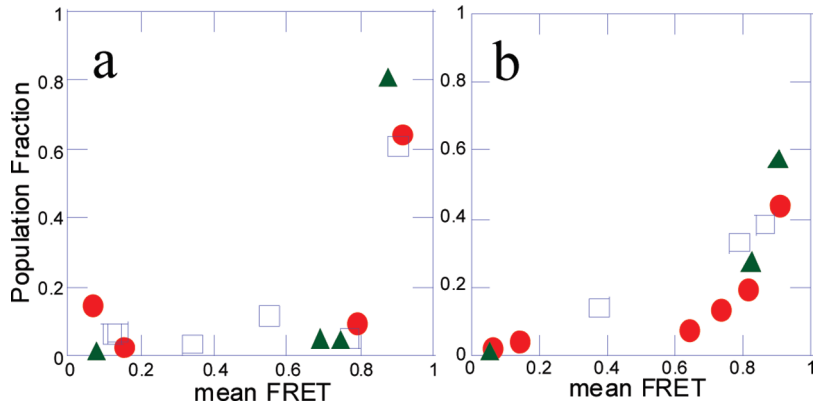


**Figure 5.** Population fraction of each conformational state found from the fits shown in Figure 4. Each conformational state is represented by its mean FRET efficiency. The solid green triangles are at 30 °C, the blue open squares are at 40 °C, and the solid red circles are at 50 °C. Graph a is under low salt (0.1 mM) conditions, and graph b depicts data taken with 57 mM NaCl.

**TABLE 1: Fit Parameters for Data Taken at 0.1 mM NaCl (a) and 57 mM NaCl (b)**

| $T$ °C | $A_1$ | $x_1$ | $\sigma_1$ | $A_2$ | $x_2$ | $\sigma_2$ | $A_3$ | $x_3$ | $\sigma_3$ | $A_4$ | $x_4$ | $\sigma_4$ | $A_5$ | $x_5$ | $\sigma_5$ | $A_6$ | $x_6$ | $\sigma_6$ | $A_7$ | $x_7$ | $\sigma_7$ |
|---|---|---|---|---|---|---|---|---|---|---|---|---|---|---|---|---|---|---|---|---|---|
| (a) Fit Parameters for Data Taken at 0.1 mM NaCl | | | | | | | | | | | | | | | | | | | | | |
| 30 | 0.03 | 0.88 | 0.054 | 0.0039 | 0.75 | 0.025 | 0.0013 | 0.69 | 0.075 | | | | | | | | | | 0.0011 | 0.078 | 0.027 |
| 40 | 0.023 | 0.90 | 0.056 | 0.0030 | 0.77 | 0.033 | | | | 0.0024 | 0.55 | 0.095 | 0.0017 | 0.34 | 0.038 | 0.0024 | 0.14 | 0.056 | 0.0091 | 0.12 | 0.014 |
| 50 | 0.025 | 0.92 | 0.055 | 0.0022 | 0.79 | 0.089 | | | | | | | | | | 0.0014 | 0.16 | 0.038 | 0.011 | 0.068 | 0.027 |
| (b) Fit Parameters for Data Taken at 57 mM NaCl | | | | | | | | | | | | | | | | | | | | | |
| 30 | 0.02 | 0.90 | 0.056 | 0.0059 | 0.82 | 0.095 | | | | | | | | | | | | | 0.0012 | 0.055 | 0.025 |
| 40 | 0.0088 | 0.86 | 0.094 | 0.0058 | 0.79 | 0.12 | | | | | | | 0.0015 | 0.38 | 0.19 | | | | | | |
| 50 | 0.014 | 0.91 | 0.069 | 0.011 | 0.82 | 0.035 | 0.006 | 0.74 | 0.045 | 0.0015 | 0.64 | 0.1 | | | | 0.001 | 0.14 | 0.09 | 0.0018 | 0.065 | 0.027 |

**TABLE 2: Dwell Times (in seconds): (a) Data Taken at 0.1 mM NaCl; (b) Data Taken at 57 mM NaCl**

| $T$ (°C) | $t_1$ | $t_2$ | $t_3$ | $t_4$ | $t_5$ | $t_6$ | $t_7$ |
|---|---|---|---|---|---|---|---|
| (a) Data Taken at 0.1 mM NaCl | | | | | | | |
| 30 | 0.29 | 0.02 | 0.01 | | | | 0.16 |
| 40 | 0.28 | 0.03 | | 0.06 | 0.04 | 0.07 | 0.06 |
| 50 | 0.67 | 0.03 | | | | 0.07 | 0.07 |
| (b) Data Taken at 57 mM NaCl | | | | | | | |
| 30 | 0.28 | 0.04 | | | | | 0.19 |
| 40 | 0.13 | 0.06 | | | 0.09 | | |
| 50 | 0.15 | 0.03 | 0.02 | <0.01 | | 0.08 | 0.07 |

as either a single conformational state or the average of a fast kinetic state.

Under all observed conditions, we have found that there are always two distinct states at the high end of the FRET efficiency histogram. This is consistent with spontaneous base flipping[13−16,18] in which the hydrogen bond between the bases is broken and the free bases form hydrogen bonds with ambient water molecules. The bases near the ends of the DNA are most likely to undergo such base-flipping, and our fluorophore probes, placed on the ends of the DNA strands, are highly sensitive to the resulting changes in distance.

## 5. Conclusion

In conclusion, we have observed the equilibrium dynamics of two isolated freely diffusing complementary 25 base-pair DNA strands in solution at various temperatures and salt concentrations. The duplex becomes unstable at high temperature and low salt concentration, as expected, and we have directly observed unbinding and rebinding of these unstable pairs. Under low-salinity conditions, we have found some atypical conformations that may constitute an unfolding pathway. Furthermore, our measurements have revealed that this short DNA oligo undergoes conformational fluctuations in solution, suggesting that the short oligo does not remain fixed in a B-form double helix conformation while freely diffusing.

**Acknowledgment.** We acknowledge funding from the Oak Ridge Associated Laboratories (ORAU), and the Department of Physics and Optical Science at the University of North Carolina in Charlotte. We thank Pat Moyer, Don Jacobs, and Andriy Baumketner for helpful discussions. Certain commercial equipment, instruments, or materials are identified in this paper to openly share our work and results with full disclosure. Such identification does not imply recommendation or endorsement by the authors, nor does it imply that the materials or equipment identified are necessarily the best available for the purpose.

## References and Notes

(1) Rotman, B. Measurement of Activity of Single Molecules of β-D-Galactosidase. *Proc. Natl. Acad. Sci. U.S.A.* **1961**, *47*, 1981.

(2) Lee, A. I.; Brody, J. P. Single-Molecule Enzymology of Chymotrypsin Using Water-in-Oil Emulsion. *Biophys. J.* **2005**, *88*, 4303.

(3) Guttenberg, Z.; et al. Planar chip device for PCR and hybridization with surface acoustic wave pump. *Lab Chip* **2005**, *5*, 308.

(4) Pietrini, A. V.; Luisi, P. L. Cell-free Protein Synthesis through Solubilisate Exchange in Water/Oil Emulsion Compartments. *ChemBioChem* **2004**, *5*, 1055.

(5) Hase, M.; et al. Manipulation of Cell-Sized Phospholipid-Coated Microdroplets and Their Use as Biochemical Microreactors. *Langmuir* **2007**, *23*, 348.

(6) Essevaz-Roulet, B.; Bockelmann, U.; Heslot, F. Mechanical separation of the complementary strands of DNA. *Proc. Natl. Acad. Sci. U.S.A.* **1997**, *94*, 11935.

(7) Edman, L.; Mets, U.; Rigler, R. Conformational transitions monitored for single molecules in solution. *Proc. Natl. Acad. Sci. U.S.A.* **1996**, *93*, 6710.

(8) Eggeling, C.; et al. Monitoring conformational dynamics of a single molecule by selective fluorescence spectroscopy. *Proc. Natl. Acad. Sci. U.S.A.* **1998**, *95*, 1556.

(9) Wennmalm, S.; Edman, L.; Rigler, R. R. Conformational fluctuations in single DNA molecules. *Proc. Natl. Acad. Sci. U.S.A.* **1997**, *94*, 10641.

(10) Singh-Zocchi, M.; et al. Single-molecule detection of DNA hybridization. *Proc. Natl. Acad. Sci. U.S.A.* **2003**, *100*, 7605.

(11) Mastroianni, A. J.; et al. Probing the Conformational Distributions of Subpersistence Length DNA. *Biophys. J.* **2009**, *97*, 1408.

(12) Matthew-Fen, R. S.; Das, R.; Harbury, P. A. B. Remeasuring the Double Helix. *Science* **2008**, *322*, 446.

(13) Klimasaukas, S.; et al. HhaI Methyltransferase flips its target base out of the DNA helix. *Cell* **1994**, *76*, 357.

(14) Roberts, R. J. On Base Flipping. *Cell* **1995**, *82*, 9.

(15) Roberts, R. J.; Cheng, X. Base Flipping. *Annu. Rev. Biochem.* **1998**, *67*, 181.

(16) Chen, Y. Z.; Mohan, V.; Griffey, R. H. Spontaneous base flipping in DNA and its possible role in methyltransferase binding. *Phys. Rev. E* **2000**, *62*, 1133.

(17) Mura, C.; McCammon, J. A. Molecular dynamics of a $\kappa$B DNA element: base flipping via cross-strand intercalative stacking in a microsecond-scale simulation. *Nucleic Acids Res.* **2008**, *36*, 4941.

(18) Varnai, P.; Lavery, R. Base Flipping in DNA: Pathways and Energetics Studied with Molecular Dynamic Simulations. *J. Am. Chem. Soc.* **2002**, *124*, 7272.

(19) Reiner, J. E.; et al. Optically Trapped Aqueous Droplets for Single Molecule Studies. *Appl. Phys. Lett.* **2006**, *89*, 013904.

(20) Jofre, A.; et al. Hydrosomes: Femtoliter containers for fluorescence spectroscopy studies. *Proc. SPIE—Int. Soc. Opt. Eng.* **2007**, *6644*, 66440E.

(21) Tang, J. Y.; et al. Green Fluorescent Protein in Optically Trapped Aqueous Nanodroplets. *Langmuir* **2008**, *24*, 4975.

(22) IDT Oligo Analyzer [cited 2009 June 2009]. Available from: http://www.idtdna.com/analyzer/Applications/OligoAnalyzer/.

(23) Bates, M.; Blosser, T. R.; Zhuang, X. Short-Range Spectroscopic Ruler Based on a Single-Molecule Optical Switch. *Phys. Rev. Lett.* **2005**, *94* (10), 108101–108105.

(24) Aitken, C. E.; Marshall, R. A.; Puglisi, J. D. An Oxygen Scavenging System for Improvement of Dye Stability in Single-Molecule Fluorescence Experiments. *Biophys. J.* **2008**, *94*, 1826.

(25) Hubner, C. G.; et al. Direct observation of the triplet lifetime quenching of single dye molecules by molecular oxygen. *J. Chem. Phys.* **2001**, *115*, 9619.

(26) Rasnik, I.; McKinney, S. A.; Ha, T. Nonblinking and long-lasting single-molecule fluorescence imaging. *Nat. Methods* **2006**, *3*, 891.

(27) Renn, A.; Seelig, J.; Sandoghdar, V. Oxygen-dependent photochemistry of fluorescnet dyes studied at the single molecule level. *Mol. Phys.* **2006**, *104*, 409.

(28) van Dijk, M. A.; et al. Combining optical trapping and single-molecule fluorescence spectroscopy: Enhanced photobleaching of fluorophores. *J. Phys. Chem. B* **2004**, *108*, 6479.

(29) Brau, R. R.; et al. Interlaced Optical Force-Fluorescence Measurements for Single Molecule Biophysics. *Biophys. J.* **2006**, *91*, 1069.

(30) Haran, G. Noise reduction in single molecule fluorescence trajectories of folding proteins. *Chem. Phys.* **2004**, *307*, 137.

(31) Deniz, A. A.; et al. Single-pair fluorescence resonance energy transfer on freely diffusing molecules: Observation of Forster distance dependence and subpopulations. *Proc. Natl. Acad. Sci. U.S.A.* **1999**, *96*, 3670.

(32) Ha, T. J.; et al. Single-molecule fluorescence spectroscopy of enzyme conformational dynamics and cleavage mechanism. *Proc. Natl. Acad. Sci. U.S.A.* **1999**, *96*, 893.

(33) Lee, N. K.; et al. Accurate FRET Measurements within Single Diffusing Biomolecules Using Alternating-Laser Excitation. *Biophys. J.* **2005**, *88*, 2939.

(34) Sniden, R. R. *DNA Structure and Function*; Academic Press: San Diego, CA, 1994; p 398.

(35) Tan, Z.-J.; Chen, S.-J. Nucleic Acid Helix Stability: Effects of Salt Concentration, Cation Valence and Size, and Chain Length. *Biophys. J.* **2006**, *90*, 1175–1190.

JP1032146